

| REPORT DOCUMENTATION PAGE   |                   |                                  | Form Approved OMB NO. 0704-0188                          |  |                                       |
|---|-------------------|----------------------------------|--|--|---------------------------------------|
| <p>The public reporting burden for this collection of information is estimated to average 1 hour per response, including the time for reviewing instructions, searching existing data sources, gathering and maintaining the data needed, and completing and reviewing the collection of information. Send comments regarding this burden estimate or any other aspect of this collection of information, including suggestions for reducing this burden, to Washington Headquarters Services, Directorate for Information Operations and Reports, 1215 Jefferson Davis Highway, Suite 1204, Arlington VA, 22202-4302. Respondents should be aware that notwithstanding any other provision of law, no person shall be subject to any penalty for failing to comply with a collection of information if it does not display a currently valid OMB control number.</p> <p>PLEASE DO NOT RETURN YOUR FORM TO THE ABOVE ADDRESS.</p> |                   |                                  |  |  |                                       |
| 1. REPORT DATE (DD-MM-YYYY)<br>31-03-2010   |                   | 2. REPORT TYPE<br>Final Report   |  | 3. DATES COVERED (From - To)<br>1-Jun-2008 - 31-Dec-2009 |                                       |
| 4. TITLE AND SUBTITLE<br>Finite-Element Simulation for Electrothermal Characterization of High-Power Diode Laser Bars   |                   |                                  | 5a. CONTRACT NUMBER<br>W911NF-08-1-0191                  |  |                                       |
|   |                   |                                  | 5b. GRANT NUMBER   |  |                                       |
|   |                   |                                  | 5c. PROGRAM ELEMENT NUMBER<br>7720AI                     |  |                                       |
| 6. AUTHORS<br>Weston T. Hobdy, Jordan M. Berg, Darryl James, Ayrton Bernussi, Luis Grave de Peralta   |                   |                                  | 5d. PROJECT NUMBER                                       |  |                                       |
|   |                   |                                  | 5e. TASK NUMBER  |  |                                       |
|   |                   |                                  | 5f. WORK UNIT NUMBER                                     |  |                                       |
| 7. PERFORMING ORGANIZATION NAMES AND ADDRESSES<br>Texas Technical University<br>203 Holden Hall<br>Box 41035<br>Lubbock, TX 79409 -1035   |                   |                                  | 8. PERFORMING ORGANIZATION REPORT NUMBER                 |  |                                       |
| 9. SPONSORING/MONITORING AGENCY NAME(S) AND ADDRESS(ES)<br>U.S. Army Research Office<br>P.O. Box 12211<br>Research Triangle Park, NC 27709-2211   |                   |                                  | 10. SPONSOR/MONITOR'S ACRONYM(S)<br>ARO                  |  |                                       |
|   |                   |                                  | 11. SPONSOR/MONITOR'S REPORT NUMBER(S)<br>54639-EL-DRP.1 |  |                                       |
| 12. DISTRIBUTION AVAILABILITY STATEMENT<br>Approved for Public Release; Distribution Unlimited  |                   |                                  |  |  |                                       |
| 13. SUPPLEMENTARY NOTES<br>The views, opinions and/or findings contained in this report are those of the author(s) and should not be construed as an official Department of the Army position, policy or decision, unless so designated by other documentation.   |                   |                                  |  |  |                                       |
| 14. ABSTRACT<br>Simulation of semiconductor diode laser performance involves interaction between multiple physics domains. This report presents the governing equations and finite-element (FE) implementation of such a simulation, including coupled calculation of electronic band structure, determined by solving Schrodinger's equation; carrier distribution and potential in the active region, solved using a drift-diffusion model; electrostatic potential in the ohmic regions, governed by Laplace's equation; temperature distribution, governed by Fourier's law and the heat equation; and  |                   |                                  |  |  |                                       |
| 15. SUBJECT TERMS<br>diode laser, semiconductor laser, simulation, high-power diode laser, finite-element simulation  |                   |                                  |  |  |                                       |
| 16. SECURITY CLASSIFICATION OF:   |                   | 17. LIMITATION OF ABSTRACT<br>UU | 15. NUMBER OF PAGES                                      | 19a. NAME OF RESPONSIBLE PERSON<br>Jordan Berg           |                                       |
| a. REPORT<br>UU   | b. ABSTRACT<br>UU |                                  |  | c. THIS PAGE<br>UU                                       | 19b. TELEPHONE NUMBER<br>806-742-3563 |

## Report Title

Finite-Element Simulation for Electrothermal Characterization of High-Power Diode Laser Bars

### ABSTRACT

Simulation of semiconductor diode laser performance involves interaction between multiple physics domains. This report presents the governing equations and finite-element (FE) implementation of such a simulation, including coupled calculation of electronic band structure, determined by solving Schrodinger's equation; carrier distribution and potential in the active region, solved using a drift-diffusion model; electrostatic potential in the ohmic regions, governed by Laplace's equation; temperature distribution, governed by Fourier's law and the heat equation; and light propagation, described by Maxwell's equations. Preliminary simulation results are provided for stripe lasers based on the GaAs/AlGaAs material system, including asymmetrically waveguided devices. Important implementation issues are discussed, particularly computation across multiple length scales and formulation of appropriate boundary conditions. Simulation results are compared to previous calculations reported in the literature. Advancement of the technical component is paralleled by development of a graphical user interface for ease of use by non-experts in FE methods.

---

**List of papers submitted or published that acknowledge ARO support during this reporting period. List the papers, including journal references, in the following categories:**

**(a) Papers published in peer-reviewed journals (N/A for none)**

Number of Papers published in peer-reviewed journals: 0.00

---

**(b) Papers published in non-peer-reviewed journals or in conference proceedings (N/A for none)**

Number of Papers published in non peer-reviewed journals: 0.00

---

**(c) Presentations**

Number of Presentations: 0.00

---

**Non Peer-Reviewed Conference Proceeding publications (other than abstracts):**

Number of Non Peer-Reviewed Conference Proceeding publications (other than abstracts): 0

---

**Peer-Reviewed Conference Proceeding publications (other than abstracts):**

Number of Peer-Reviewed Conference Proceeding publications (other than abstracts): 0

---

**(d) Manuscripts**

Number of Manuscripts: 0.00

---

Number of Inventions:

---

Graduate Students

| <u>NAME</u>            | <u>PERCENT SUPPORTED</u> |
|------------------------|--------------------------|
| Weston Hobby           | 1.00                     |
| Deepak Malleshappa     | 0.25                     |
| Uday Narayanappa       | 0.10                     |
| Nenad Stojanovic       | 0.08                     |
| <b>FTE Equivalent:</b> | <b>1.43</b>              |
| <b>Total Number:</b>   | <b>4</b>                 |

**Names of Post Doctorates**

| <u>NAME</u>            | <u>PERCENT SUPPORTED</u> |
|------------------------|--------------------------|
| <b>FTE Equivalent:</b> |                          |
| <b>Total Number:</b>   |                          |

**Names of Faculty Supported**

| <u>NAME</u>            | <u>PERCENT SUPPORTED</u> | National Academy Member |
|------------------------|--------------------------|-------------------------|
| Darryl James           | 0.08                     | No                      |
| Jordan M. Berg         | 0.08                     | No                      |
| <b>FTE Equivalent:</b> | <b>0.16</b>              |                         |
| <b>Total Number:</b>   | <b>2</b>                 |                         |

**Names of Under Graduate students supported**

| <u>NAME</u>            | <u>PERCENT SUPPORTED</u> |
|------------------------|--------------------------|
| <b>FTE Equivalent:</b> |                          |
| <b>Total Number:</b>   |                          |

**Student Metrics**

This section only applies to graduating undergraduates supported by this agreement in this reporting period

- The number of undergraduates funded by this agreement who graduated during this period: ..... 0.00
- The number of undergraduates funded by this agreement who graduated during this period with a degree in science, mathematics, engineering, or technology fields:..... 0.00
- The number of undergraduates funded by your agreement who graduated during this period and will continue to pursue a graduate or Ph.D. degree in science, mathematics, engineering, or technology fields:..... 0.00
- Number of graduating undergraduates who achieved a 3.5 GPA to 4.0 (4.0 max scale):..... 0.00
- Number of graduating undergraduates funded by a DoD funded Center of Excellence grant for Education, Research and Engineering:..... 0.00
- The number of undergraduates funded by your agreement who graduated during this period and intend to work for the Department of Defense ..... 0.00
- The number of undergraduates funded by your agreement who graduated during this period and will receive scholarships or fellowships for further studies in science, mathematics, engineering or technology fields:..... 0.00

**Names of Personnel receiving masters degrees**

| <u>NAME</u>          |
|----------------------|
| Weston Hobby         |
| <b>Total Number:</b> |

1

---

**Names of personnel receiving PHDs**

NAME

**Total Number:**

---

**Names of other research staff**

NAME

PERCENT SUPPORTED

Vladimir Kuryatkov

0.08 No

**FTE Equivalent:**

**0.08**

**Total Number:**

**1**

---

**Sub Contractors (DD882)**

**Inventions (DD882)**

Section: Scientific Progress and  
Accomplishments

Report Type: Final Report

Proposal Number: 54639ELDRP

Agreement Number: W911NF0810191

Proposal Title: Finite-Element Simulation for  
Electrothermal Characterization of  
High-Power Diode Laser Bars

# Contents

|          |  |           |
|----------|--|-----------|
| <b>1</b> | <b>Introduction: Multiphysics Modeling</b>             | <b>1</b>  |
| <b>2</b> | <b>Electrothermal Model</b>                            | <b>1</b>  |
| 2.1      | Drift-Diffusion Model . . . . .                        | 3         |
| 2.1.1    | Carrier Concentrations . . . . .                       | 4         |
| 2.2      | Conduction Heat Transfer Model . . . . .               | 5         |
| 2.3      | Boundary Conditions for Electrothermal Model . . . . . | 6         |
| <b>3</b> | <b>Recombination Mechanisms</b>                        | <b>7</b>  |
| 3.1      | Stimulated Recombination . . . . .                     | 8         |
| 3.1.1    | Optical Gain . . . . .                                 | 8         |
| 3.1.2    | Photon Group Velocity . . . . .                        | 10        |
| 3.1.3    | Photon Density . . . . .                               | 10        |
| 3.2      | Spontaneous Recombination . . . . .                    | 11        |
| 3.3      | Nonradiative Recombination . . . . .                   | 12        |
| <b>4</b> | <b>Optical Model</b>                                   | <b>12</b> |
| 4.1      | Calculation of Optical Mode . . . . .                  | 13        |
| 4.2      | Asymmetric Waveguiding: SHEDS Lasers . . . . .         | 14        |
| <b>5</b> | <b>Eigenenergy Calculation</b>                         | <b>15</b> |
| <b>6</b> | <b>Conclusion</b>                                      | <b>17</b> |
|          | <b>Nomenclature</b>                                    | <b>19</b> |
|          | <b>References</b>                                      | <b>22</b> |

## List of Figures

|   |   |    |
|---|---|----|
| 1 | Schematic illustrating the coupling between physical domains in semiconductor lasers. . . . . | 2  |
| 2 | Contour plot of temperature over a mirrored facet of a high powered diode laser. . . . .      | 3  |
| 3 | Boundary conditions for the electrothermal model. . . . .                                     | 7  |
| 4 | Material gain as a function of photon energy . . . . .  | 10 |
| 5 | Spontaneous emission rate as a function of photon energy . . .                                | 12 |
| 6 | Optical mode distribution for symmetric waveguide. . . . .                                    | 14 |
| 7 | Optical mode distribution for an asymmetric waveguide. . . .                                  | 15 |
| 8 | Graphical representation of the solution to Schrödinger's equation. . . . .                   | 17 |
| 9 | Allowed electron eigenenergies plotted with conduction band profile. . . . .                  | 18 |

## **Abstract**

Simulation of semiconductor diode laser performance involves interaction between multiple physics domains. This report presents the governing equations and finite-element (FE) implementation of such a simulation, including coupled calculation of electronic band structure, determined by solving Schrödinger's equation; carrier distribution and potential in the active region, solved using a drift-diffusion model; electrostatic potential in the ohmic regions, governed by Laplace's equation; temperature distribution, governed by Fourier's law and the heat equation; and light propagation, described by Maxwell's equations. Preliminary simulation results are provided for stripe lasers based on the GaAs/AlGaAs material system, including asymmetrically waveguided devices. Important implementation issues are discussed, particularly computation across multiple length scales and formulation of appropriate boundary conditions. Simulation results are compared to previous calculations reported in the literature. Advancement of the technical component is paralleled by development of a graphical user interface for ease of use by non-experts in FE methods.

# 1 Introduction: Multiphysics Modeling

At the most fundamental level, the generation and characteristics of the light produced by a semiconductor laser is due to the quantum mechanical interaction of electrons, holes, photons, and phonons. Therefore, electronics, optics, and temperature ultimately determine the performance of a laser diode. The magnitude of injection current needed to operate a high powered laser diode results in high temperatures, reducing the external efficiency and operating lifetime. A comprehensive simulation models the coupling of optics, temperature, and electronics in a self-consistent manner. However, such comprehensive models often face numerous computational problems. One such problem is due to the multiple length scales in a laser structure. The thicknesses of the layers in a given diode vary between several orders of magnitude. For example, the thickness of the substrate is typically on the order of a hundred microns, whereas the thickness of the quantum well is less than ten nanometers. In thick layers, classical characteristics dominate the behavior of carriers. However, in the quantum well, the band structure becomes quantized in energy. Further, the radical differences in the layer thicknesses leads to computationally taxing simulations, owing to the mesh densities required for an accurate solution. Therefore, a useful simulation must capture the essential physical phenomena and simultaneously be numerically tractable for the computational hardware available. We have developed a preliminary graphical user interface that makes use of the Matlab scripting options in COMSOL Multiphysics. This allows the user to perform simulations without expertise in the finite-element method and still maintain control over the device geometry and composition.

## 2 Electrothermal Model

The electrothermal model solves for the potential and temperature fields, models the electron and hole transport. Ultimately, the current-voltage (IV) characteristics of the diode are given by the transport model. Because of the interaction between the drift and diffusion of carriers, the IV characteristics are non-Ohmic or nonlinear. Joule, or resistive, heating depends on both the current density and the electric field; and the Fermi-Dirac distributions that determine the nonequilibrium carrier densities depend on temperature. Therefore, the temperature field is strongly coupled to the electron-hole transport model. The default simulation structure throughout this report is similar to the one presented in [17]. A contour plot of the temperature over a mirrored facet of the laser is shown in Fig. 2.

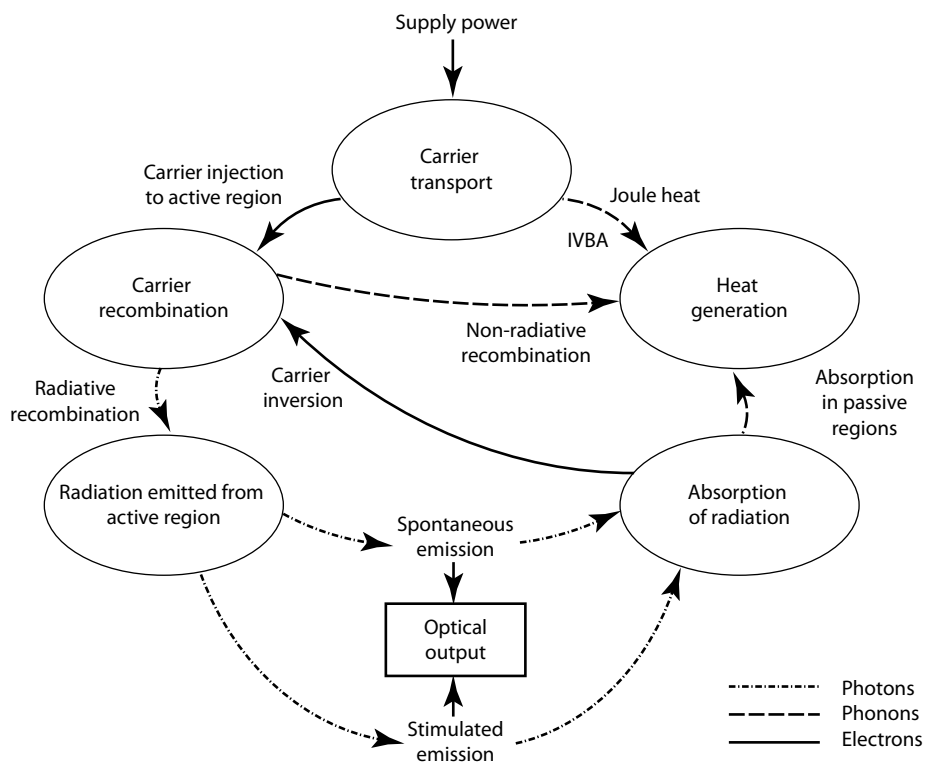


Figure 1: Schematic illustrating the coupling between physical domains in semiconductor lasers.

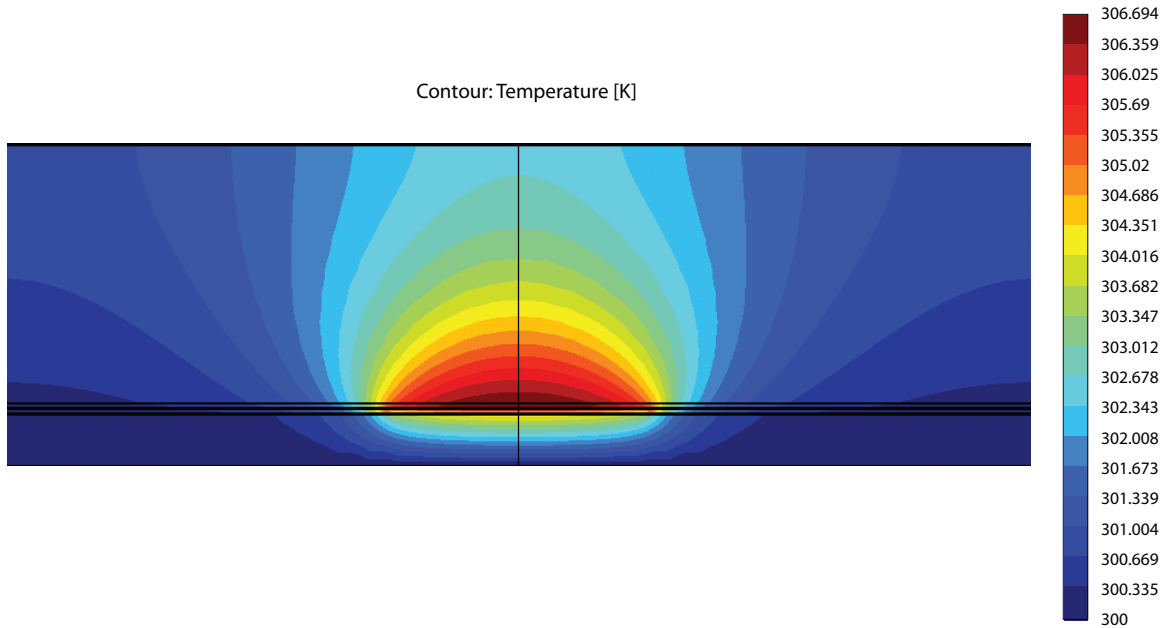


Figure 2: Contour plot of temperature over a mirrored facet of a high powered diode laser.

Optical heating is due to the absorption of photons by free carriers, and therefore depends on the photon and free carrier densities [21]. Optical heating is not modeled in the present work, but is particularly important in long wavelength lasers emitting around  $1.55 \mu\text{m}$  [2].

## 2.1 Drift-Diffusion Model

The drift-diffusion equations are used to model the transport of electrons and holes through the device. The nomenclature of the equations results from the phenomena they model: carrier drift, due to the electric field; and carrier diffusion, due to concentration gradients. The electrostatic potential is determined by the solution to Poisson's equation,

$$\nabla \cdot (-\varepsilon \nabla \psi) = q(p - n + N) \quad (1)$$

where  $\psi$  is the electrostatic potential,  $\varepsilon = \varepsilon_s \varepsilon_0$  is the permittivity,  $q$  the electron charge,  $p$  the hole concentration,  $n$  the electron concentration, and  $N = N_D^+ - N_A^-$  the doping profile. The model assumes the full ionization of dopants.

Further, the drift-diffusion equations solve for the electron and hole contributions to the current density. The current densities are determined by

continuity equations that balance the flux of carriers through a control volume with the rate at which carriers recombine. For electrons, that is,

$$\frac{\partial n}{\partial t} = \frac{1}{q} \nabla \cdot \mathbf{j}_n - \sum R, \quad (2)$$

where  $\mathbf{j}_n$  is the electron contribution to the current density, and  $\sum R$  is the sum of the *net recombination rates*, which are defined as the recombination rates minus the generation rates. An analogous equation holds for the hole flux,

$$\frac{\partial p}{\partial t} = \frac{1}{q} \nabla \cdot \mathbf{j}_p + \sum R, \quad (3)$$

where  $\mathbf{j}_p$  is the hole contribution to the hole current density. The total current density is given by the  $\mathbf{j} = \mathbf{j}_n + \mathbf{j}_p$ . The electron and hole contributions to the current density are given by the quasi-Fermi formulation of the drift-diffusion equations [29], [14]. The electron current density is calculated by,

$$\mathbf{j}_n = -qn\mu_n \nabla \varphi_n. \quad (4)$$

Similarly, the hole current density is,

$$\mathbf{j}_p = -qp\mu_p \nabla \varphi_p. \quad (5)$$

The continuity equations are implemented in steady state, so that the time derivatives are zero. The quasi-Fermi potentials are related to the quasi-Fermi energies as  $E_{Fc} = -q\varphi_n$  and  $E_{Fv} = -q\varphi_p$ . The electron and hole mobilities are given by  $\mu_n$  and  $\mu_p$ , respectively. The calculation of carrier mobility varies in complexity, ranging from simple, constant, low-field mobilities; to computationally-taxing molecular dynamics simulations. Since the current densities are directly proportional to the mobility, it is important that it be accurately determined. Additionally, the mobility must be computationally tractable in a reasonable time, and should reflect the dependence of mobility on temperature. The mobilities in the present work are calculated using the semi-empirical, Caughey-Thomas-like parameters given in [27]. The mobility model gives the dependence of temperature and doping, and is well-suited for device simulation.

### 2.1.1 Carrier Concentrations

In general, the carrier concentrations can be determined by integrating the density of states and occupation functions over all energies in a energy band, such as

$$n = \int_{E_c}^{\infty} \rho_c(E) f_c(E) dE \quad (6)$$

for the conduction band, where  $E_c$  is the conduction band minimum,  $\rho_c$  is the density of states function, and  $f_c$  is the Fermi-Dirac function for the conduction band. A significant simplification can be made by assuming non-degenerate doping levels [5]. This assumption is justified if the doping is such that the equilibrium Fermi energy  $E_F$  is at least  $3k_B T$  less than the conduction band minimum, and at least  $3k_B T$  greater than the valence band maximum. Under these conditions, the Fermi-Dirac distribution approaches the Maxwell-Boltzmann distribution, and the bulk carrier density can be calculated from the quasi-Fermi energies without the need for integration, as

$$n = n_i \exp [q(\psi - \varphi_n) / (k_B T)] = N_c \exp [(E_{Fc} - E_c) / (k_B T)], \quad (7)$$

and

$$p = n_i \exp [q(\varphi_p - \psi) / (k_B T)] = N_v \exp [(E_v - E_{Fv}) / (k_B T)], \quad (8)$$

where  $N_c$  and  $N_v$  are the effective density of states for the conduction and valence bands, respectively. These are given by  $N_c = 2 [2\pi m_c^* k_B T / h^2]^{3/2}$  and  $N_v = 2 [2\pi m_v^* k_B T / h^2]^{3/2}$ , where  $m_v^* = (m_{lh}^{*3/2} + m_{hh}^{*3/2})^{2/3}$  for light and heavy holes [14], [5]. The equalities above, wherein the carrier density is a function of the quasi-Fermi energy, are useful in the calculation of the recombination rates, which depend on the quasi-Fermi energies relative to the band extrema.

The above carrier density calculation is valid in the bulk. However, quantization of the energy bands leads to a different density of states function for carriers with energy less than the quantum well barrier energy. Additionally, some carriers may have energy greater than the quantum well barrier; these carriers obey the bulk carrier density equations (7) and (8). The total carrier density calculated at the quantum well is the sum of these two. The density of bound carriers in the quantum well is given by [18], [7] as

$$n_{\text{bound}} = \frac{m_c^* k_B T}{\pi \hbar^2 d_a} \sum_n \ln \{1 + \exp [-(E_{cn} - E_{Fc}) / (k_B T)]\}, \quad (9)$$

where the summation is over the bound states computed in Section 5. An analogous equation is used for bound holes.

## 2.2 Conduction Heat Transfer Model

The temperature field is computed using Fourier's law and the heat equation. The present model considers only Joule heating, although optical heating has proven to be significant in some material systems, particularly InGaAsP-based, long wavelength lasers [21]. The heat equation is,

$$\nabla \cdot (-\kappa \nabla T) = q_{Joule}''' \quad (10)$$

where  $\kappa$  is the thermal conductivity,  $T$  is the lattice temperature. The Joule heating term is calculated using,

$$q_{Joule}''' = -\mathbf{j} \cdot \nabla \psi. \quad (11)$$

### 2.3 Boundary Conditions for Electrothermal Model

The boundary conditions for the electrothermal model are shown in Fig. 3. Far from the depletion regions at the device contacts, it is reasonable to assume that the carrier concentrations relax to their equilibrium values ([4], pg 313; [1]). The potential will also be at its equilibrium value  $\psi_0$  on the n-contact, calculated by eq. (12). If the device is in forward bias with applied voltage  $V_a$ , the p-contact will be at a potential of  $\psi_0 + V_a$ . In the framework of quasi-Fermi levels, this implies that the quasi-Fermi energies far from the junction return to the equilibrium Fermi level  $E_F$ , which describes the equilibrium carrier statistics. If the Fermi potential ( $\varphi_F = -E_F/q$ ) is used as the reference, it may be shown that the n-contact uses the Dirichlet conditions  $\varphi_n = 0$ ,  $\varphi_p = 0$ , and  $\psi = \psi_0$ . The p-doped contact uses the Dirichlet conditions  $\varphi_n = V_a$ ,  $\varphi_p = V_a$ , and  $\psi = \psi_0 + V_a$ . The metal-semiconductor interface physics are not modeled because the semiconductor materials near the n- and p-contacts are heavily doped ( $n^+$  and  $p^+$ ) to prevent a large voltage drop across this barrier (pg. 175 of [9]). It is also worth noting that the applied voltage must be gradually increased from zero in increments of approximately  $k_B T/q \approx 0.026$  V (at room temperature) until the desired potential is reached [29].

The equilibrium potential distribution is a result of the diffusion of carriers across the p-n junction, which sets up an electric field. The equilibrium potential distribution is computed with [1],

$$\psi_0 = \frac{k_B T}{q} \left( \ln \left[ \frac{n_{N0}}{n_i} \right] + \ln \left[ \frac{p_{P0}}{n_i} \right] \right), \quad (12)$$

with equilibrium electron concentration in the n-doped region,

$$n_{N0} = \frac{|N| + \sqrt{N^2 + 4n_i^2}}{2}, \quad (13)$$

and equilibrium hole concentration in the p-doped region,

$$p_{P0} = \frac{|N| + \sqrt{N^2 + 4n_i^2}}{2}. \quad (14)$$

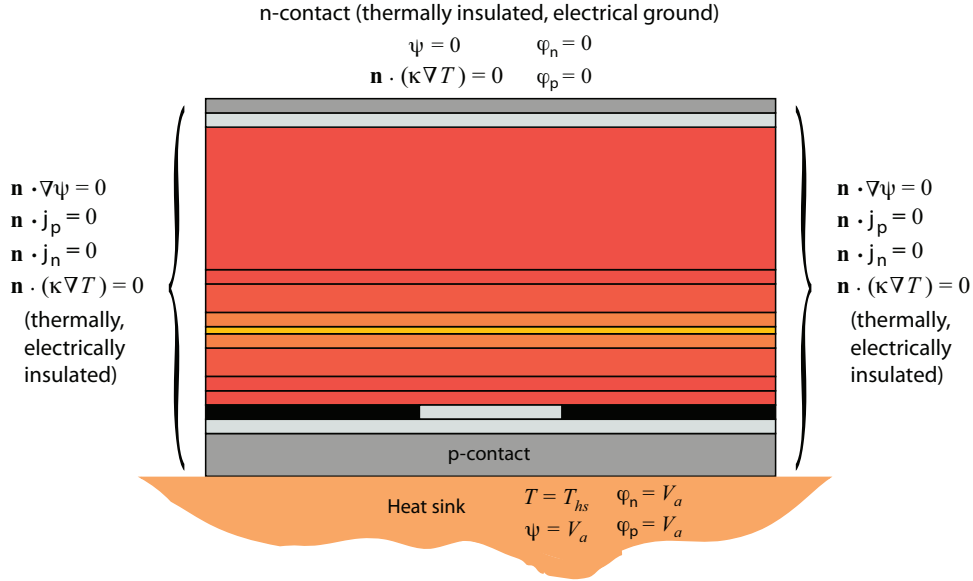


Figure 3: Boundary conditions for the electrothermal model. The p-contact is attached to an ideal heat sink at  $T = T_{hs}$ , and at drive voltage  $\psi = \psi_0 + V_a$ . The n-contact is thermally insulated, and serves as electrical ground.

The thermal boundary condition over the top contact has been investigated experimentally [28] and it was determined that due to the presence of a metal electrical contact, the boundary should be modeled as isothermal, rather than convective or insulated. This is naturally accounted for in our model, since the metal contact included in the simulation has high thermal conductivity and therefore facilitates a uniform heat distribution. All other boundaries are thermally insulated, with the exception of the boundary in contact with the heat sink, which uses the Dirichlet boundary condition  $T = T_{hs}$  to account for the heat sink temperature. This models the heat sink as ideal.

### 3 Recombination Mechanisms

The process by which an electron in the conduction band falls into an empty state in the valence band is known as recombination. The potential energy lost by the electron during recombination is manifested in another form. In the event that the energy is transformed to light, by the emission of a photon, the process is known as radiative recombination. Stimulated and spontaneous recombination are radiative recombination mechanisms. All other processes are loosely termed nonradiative recombination. Nonradiative recombination

can result in the creation of phonons, through Shockley-Read-Hall recombination; or the energy can be kinetic energy imparted to an electron or hole, by way of Auger recombination (pg. 193-194 of [5]).

### 3.1 Stimulated Recombination

The key feature in the operation of a semiconductor is stimulated emission via optical gain. Optical gain is achieved by the condition of population inversion, wherein electrons are stimulated to the conduction band, leaving holes in the valence band. Population inversion occurs when the potential across the quantum well leads to a quasi-Fermi level separation greater than the band gap [9], [7]. When population inversion has been achieved, optical gain occurs by the interaction of the electromagnetic field with the electron-hole pairs, leading to recombination which emits a photon of the same frequency as the perturbing electromagnetic field. Optical gain gives the increase per unit length in the number of photons, and thus its calculation depends on the quasi-Fermi energy separation determined by the drift-diffusion model. The stimulated emission rate (in units of per unit volume per unit time) is related to the optical gain by,

$$R_{st} = v_g g N_{ph} \quad (15)$$

where  $v_g$  is the group velocity and  $N_{ph}$  the photon density. The calculation of these parameters is discussed in the subsequent subsections.

#### 3.1.1 Optical Gain

Optical gain is defined as the proportional increase in the photon density per unit length of active material. Parabolic band shapes and  $k$ -selection rules are assumed. The expression for the optical gain as a function of the photon energy is [3], [30], ch. 1 and 2 of [18],

$$g(E_i) = \frac{\pi q^2 \hbar n_{g,\text{eff}}}{\varepsilon_0 m_0^2 c_0 n_r^2 E_i} \sum_j \sum_n \int_{E_g + E_{cn} + E_{jn}}^{\infty} |M_{QW}|^2 \rho_{red,j}(E) (f_{cn,j} - f_{vn,j}) \mathcal{L}(E) dE. \quad (16)$$

Here,  $c_0$  is the speed of light in a vacuum,  $m_0$  is the free electron mass,  $n_r$  is the refractive index,  $n_{g,\text{eff}}$  is the group effective refractive index,  $E_i$  is the photon energy, and  $j = hh, lh$  for heavy holes and light holes, respectively.  $|M_{QW}|^2$  is the squared transition matrix element for a quantum well given by [30],

$$|M_{QW}|^2 = \frac{3}{4} |M_{avg}|^2 \left[ 1 + \frac{E_{cn}}{E_{cn} + \frac{m_{red,j}^*}{m_c^*} (E - E_g - E_{cn} - E_{jn})} \right], \quad (17)$$

with

$$|M_{avg}|^2 = \frac{m_0}{6} \left( \frac{m_0}{m^*} - 1 \right) \frac{E_g (E_g + \Delta)}{E_g + 2\Delta/3}. \quad (18)$$

$m^*$  is a modified effective mass that takes account for higher and lower conduction bands (taken to be  $0.053m_0$  in GaAs),  $\Delta$  is the spin-orbit splitting energy, and  $E_g$  is the band gap. The derivation of  $|M_{avg}|^2$  assumes that a single factor of two is included in the reduced density of states to account for spin degeneracy [30]. The reduced density of states function, including the factor of two for spin degeneracy, is given by [18], [20],

$$\rho_{red,j}(E) = \frac{4\pi m_{red,j}^*}{h^2 d_a} \mathcal{H}(E - E_g - E_{cn} - E_{jn}) \quad (19)$$

where  $\mathcal{H}$  is the Heaviside unit step function. The reduced effective mass is given by,

$$m_{red,j}^* = \frac{m_c^* m_j^*}{m_c^* + m_j^*}, \quad (20)$$

and the modified Fermi distribution for conduction band states is given by,

$$f_{cn,j} = \left\{ 1 + \exp \left[ \left( E_{cn} + \frac{m_{red,j}^*}{m_c^*} (E - E_g - E_{cn} - E_{jn}) - E_{Fc} \right) / (k_B T) \right] \right\}^{-1}, \quad (21)$$

and the modified Fermi distribution for valence band states is given by,

$$f_{vn,j} = \left\{ 1 + \exp \left[ \left( -E_{vn} - \frac{m_{red,j}^*}{m_j^*} (E - E_g - E_{cn} - E_{jn}) - E_{Fv} \right) / (k_B T) \right] \right\}^{-1}. \quad (22)$$

Lastly, the spectral broadening function is a simple Lorentzian distribution, given by [18] as,

$$\mathcal{L}(E) = \frac{1}{\pi} \frac{\hbar/\tau_{in}}{(E - E_i)^2 + (\hbar/\tau_{in})^2}, \quad (23)$$

where  $\tau_{in}$  is the intraband relaxation time, typically taken to be 0.1 ps [3], [18]. Intraband relaxation or spectral broadening takes account for the uncertainty in the energy states [7]. The material gain spectrum is plotted as as function of photon energy in Fig. 4.

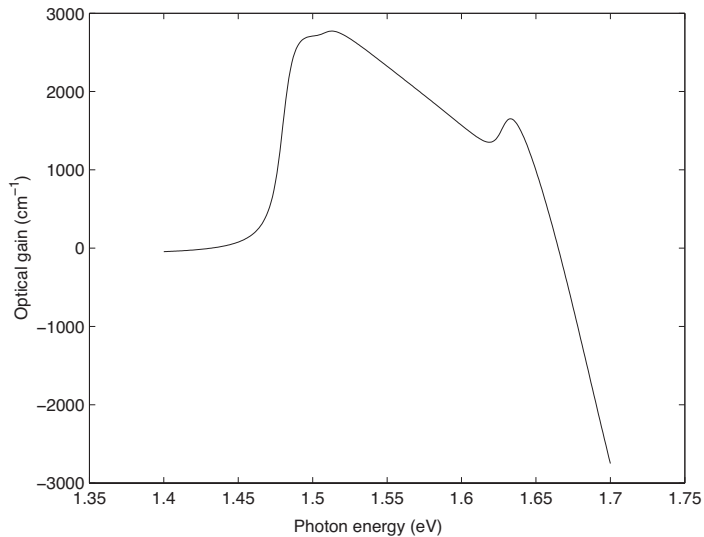


Figure 4: Material gain as a function of photon energy for 8 nm GaAs single quantum well device with a carrier concentration of  $10^{19} \text{ cm}^{-3}$ .

### 3.1.2 Photon Group Velocity

The photon group velocity is defined as [9], [18]

$$v_g = \frac{c_0}{n_{g,\text{eff}}}, \quad (24)$$

where  $c_0$  is the speed of light in a vacuum, and  $n_{g,\text{eff}}$  is the group effective refractive index, which is given approximately by,

$$n_{g,\text{eff}} \approx n_{r,\text{eff}} - \frac{\partial n_{r,\text{eff}}}{\partial \lambda_0} \lambda_0, \quad (25)$$

The group refractive index is found by using a forward difference approximation to  $\partial n_{r,\text{eff}} / \partial \lambda_0$ .

### 3.1.3 Photon Density

The number of photons per unit volume in the cavity is determined by an energy balance written for the optical cavity. The equation balances the contributions of stimulated emission, spontaneous emission, and the rate of photon loss via the mirror and internal losses. The steady-state balance equation for the photon density in the quantum well is [9], [7], [14],

$$v_g g N_{ph} + R'_{sp} - \frac{v_g}{\Gamma} \left( \alpha_i + \frac{1}{2L} \ln \left[ \frac{1}{R_1 R_2} \right] \right) N_{ph} = 0. \quad (26)$$

The term  $R'_{sp}$  gives the spontaneous emission emitted into the lasing mode,  $\Gamma$  is the optical confinement factor,  $\alpha_i$  is the internal losses (taken to be  $\alpha_i = 5 \text{ cm}^{-1}$  [7]), and  $R_1, R_2$  are the mirror reflectivities. Solving equation 26 for  $N_{ph}$  yields,

$$N_{ph} = \frac{R'_{sp}}{v_g \left( \frac{1}{\Gamma} \left[ \alpha_i + \frac{1}{2L} \ln \left( \frac{1}{R_1 R_2} \right) \right] - g \right)} \quad (27)$$

where the spontaneous emission into the lasing mode is given by [7],

$$R'_{sp} = \frac{\Gamma v_g g n_{sp}}{V}, \quad (28)$$

where  $V$  is the quantum well volume, with the population inversion factor given by,

$$n_{sp} = \{1 - \exp [(E_i - \Delta E_F) / (k_B T)]\}^{-1}. \quad (29)$$

where  $\Delta E_F = E_{F_c} - E_{F_v}$  is the quasi-Fermi level separation.

### 3.2 Spontaneous Recombination

For injection currents below the threshold current,  $R_{sp} \gg R_{st}$ . The emitted light is of many polarizations and frequencies. Within the electrothermal drift-diffusion simulation, spontaneous emission is not modeled. However, the optical spectrum of spontaneous emission can be determined by a calculation similar to that of the optical gain spectrum. The expression used to calculate the spontaneous emission rate is [18],

$$r_{sp}(E_i) = \frac{q^2 n_r E}{\pi m_0^2 \hbar^2 c_0^3 \epsilon_0} \sum_n \sum_j |M_{avg}|^2 \rho_{red,j}(E) f_{cn,j} (1 - f_{vn,j}), \quad (30)$$

where  $n_r$  is the refractive index of the quantum well material,  $E_i$  is the photon energy, and  $|M_{avg}|^2$  is the magnitude of the energy-independent momentum matrix element, given by equation (18).

The total spontaneous emission rate is found by integrating over all photon energies [6] so that,

$$R_{sp} = \int_0^\infty r_{sp}(E) dE, \quad (31)$$

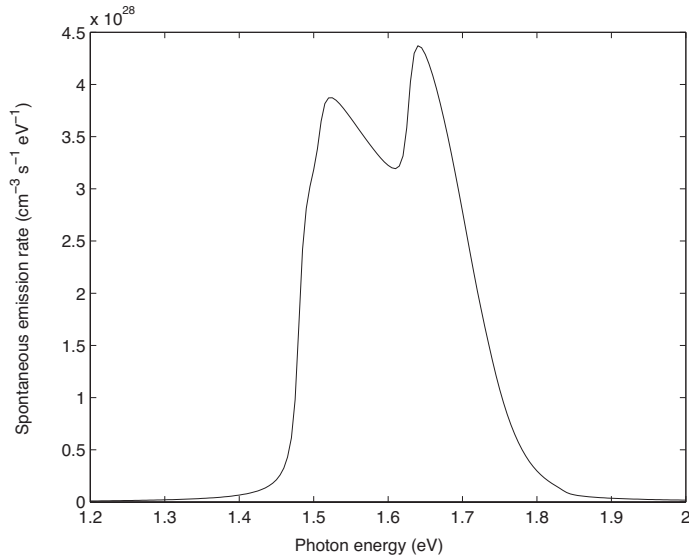


Figure 5: Spontaneous emission rate as a function of photon energy for 8 nm GaAs single quantum well device with a carrier concentration of  $10^{19} \text{ cm}^{-3}$ .

It is not necessary to convolve the spontaneous emission function with a broadening function to determine the total rate, but it is appropriate in a calculation of the spontaneous emission spectrum [18], [30], [6]. The calculated spontaneous emission spectrum is shown in Fig. 5.

### 3.3 Nonradiative Recombination

Two types of nonradiative recombination present in a laser diode are Shockley-Read-Hall (SRH) recombination and Auger recombination. SRH recombination is due to the presence of point defects, and the rate at which carriers recombine due to SRH recombination is given by, [1],

$$R_{SRH} = \frac{np - n_i^2}{\tau_p(n + n_i) + \tau_n(p + n_i)} \quad (32)$$

## 4 Optical Model

The optical model calculates the optical mode shape. The optical mode shape determines the optical confinement factor  $\Gamma$ , which describes the fraction of light that is confined to the quantum well. The remaining fraction is absorbed by the waveguiding layers and leads to optical heating. The optical model

reduces the diode geometry to the optical region, which we define as the portion of the waveguiding structure where a non-negligible portion of light is confined. This includes the n- and p-doped cores and cladding layers, and the quantum well.

## 4.1 Calculation of Optical Mode

The optical mode shape is determined by the solution of the Helmholtz equation, which is derived from Maxwell's equations,

$$\nabla^2 \mathbf{E}_0 + k_0^2 (n_r^2 - n_{r,\text{eff}}^2) \mathbf{E}_0 = 0, \quad (33)$$

where  $\mathbf{E}_0 = \mathbf{E}_0(x, y)$  is the optical mode shape,  $n_{r,\text{eff}}$  is an eigenvalue,  $k_0 = 2\pi/\lambda_0$  is the wave number in a vacuum, and  $n_r$  is the complex refractive index, which contains information about the gain or absorption coefficient,

$$n_r^2 = \left( \bar{n}_r + i \frac{g}{2k_0} \right)^2 \quad (34)$$

in the quantum well, where  $\bar{n}_r$  is the real part of the refractive index, calculated by the model presented in [10] for  $\text{Al}_x\text{Ga}_{1-x}\text{As}$ . In the passive layers, the substitution  $g \rightarrow -\alpha$  is made to account for absorption. This link is not yet implemented in the present work, because the temperature must be mapped from the electrothermal simulation to the optical model to give the temperature dependence of  $\bar{n}_r$ .

Since  $k_0$  depends on  $\lambda_0$ , Schrödinger's equation must first be solved to determine the wavelength. The Helmholtz equation is solved in the  $x$ - $y$  plane of the laser, with the wave propagating in the  $z$ -direction. The boundary conditions used to solve the optical simulation assume that the mode shape goes to zero at the boundaries of the optical region. The simulation uses a  $y$  cross-section of the fundamental waveguide mode profile and normalizes the profile such that,

$$\int_{-\infty}^{\infty} \mathbf{E}_0^2(y) dy = 1 \quad (35)$$

A normalized optical mode distribution for a symmetric waveguide is shown in Figure 6. The waveguide for the structure used to calculate Figure 6 is symmetric with respect to the geometry and the refractive indices. The optical confinement factor is defined as the overlap of the optical mode shape with the active region. That is,

$$\Gamma = \frac{\int_0^{d_a} \mathbf{E}_0^2(y) dy}{\int_{-\infty}^{\infty} \mathbf{E}_0^2(y) dy} = \int_0^{d_a} \mathbf{E}_0^2(y) dy \quad (36)$$

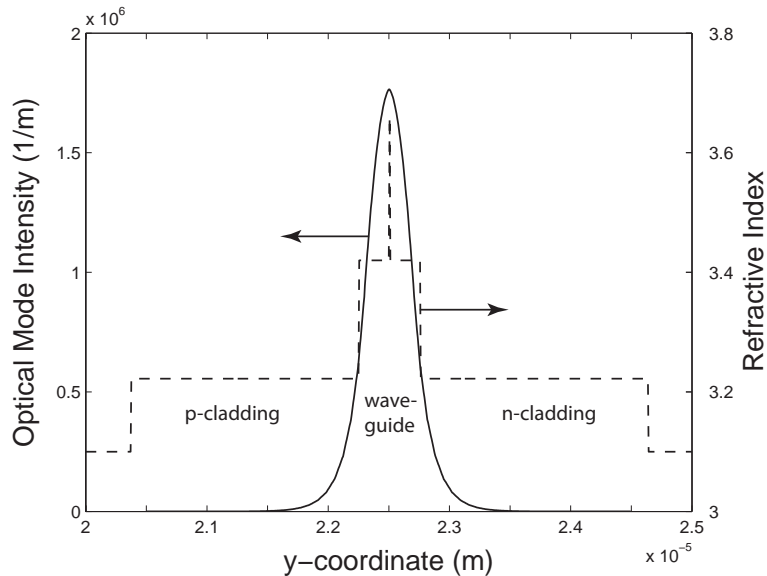


Figure 6: Normalized optical mode distribution and refractive index variation with position for a symmetric waveguide.

## 4.2 Asymmetric Waveguiding: SHEDS Lasers

Long wavelength ( $\lambda_0 = 1.55 \mu\text{m}$ ) laser structures utilizing asymmetric waveguides have been shown to be advantageous experimentally [19], [15], [13] and theoretically [26], [21], [23], [22], [24]. Such lasers are known as Super High Efficiency Diode Structures, or SHEDS lasers. The large density of free carriers in the active region of a laser diode gives rise to free carrier absorption [21] and bimolecular recombination [25] in the p- and n-doped core and cladding. These phenomena reduce the external efficiency of the laser. Free carrier absorption occurs as a result of the overlap of the optical mode shape with the highly doped cladding layers [26]. Quantum mechanical calculations have proved that the contributions to free carrier absorption by interconduction and intraconduction band absorption are negligible in laser diodes [12]. The dominant process is intervalence band absorption (IVBA) [22].

Proposed solutions to decrease the free carrier absorption include broadening the thickness of the core for better optical confinement, or using an asymmetric waveguide with respect to the position of the quantum well. The effects of the latter are explored in this section. The p-cladding is highly lossy, due to two effects: the p-material has a larger free-carrier absorption cross-section than that of the n-material, and a higher doping concentration to compensate for the low hole mobility (relative to electron mobility) [23]. Therefore, optimal designs seek to reduce the overlap of the optical mode

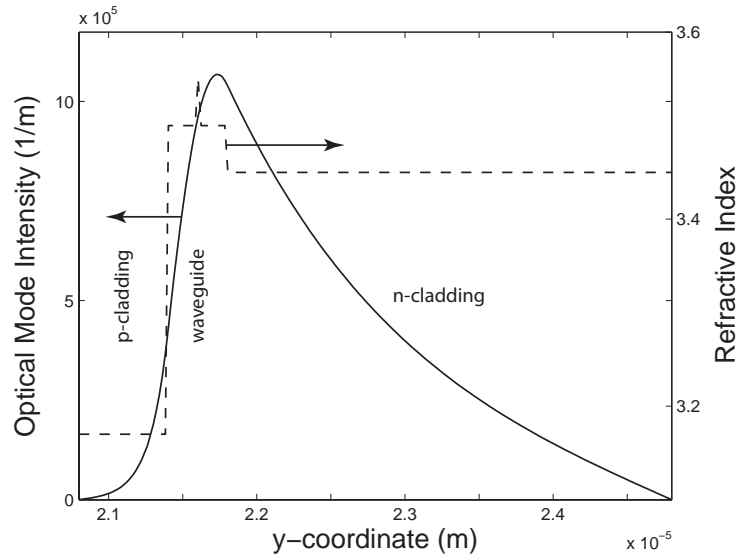


Figure 7: Normalized optical mode distribution and refractive indices for an asymmetric waveguide (geometry and material properties from [22]). Note the overlap of the optical mode with the n-cladding and reduced overlap with the p-cladding relative to the symmetric waveguide of Fig. 6.

shape with this layer. This is achieved not only by geometric asymmetry, but by index-guiding the optical mode by using a material with higher refractive index for the n-cladding relative to that of the p-cladding. Index-guiding in this manner does increase the overlap of the optical mode shape with the n-cladding. This is illustrated in Fig. 7, which uses material properties and dimensions from [22]. However, the n-cladding can be made much less lossy than the p-cladding in terms of free carrier absorption, because the higher electron mobility allows for a lower magnitude of donor doping concentration to achieve the same electrical conduction properties. The optical mode shape determines the free carrier absorption at a point, and therefore the volumetric heating term  $q_{opt}'''$ .

## 5 Eigenenergy Calculation

In the quantum well, the conduction and valence bands develop into discrete energy subbands. The calculation of the allowed subband minima follows a standard quantum mechanical treatment (see, for example, [16], [3]) for a single particle in a finite potential well. The carriers are bound to the potential well by the band energy offsets between the quantum well material

and the barrier materials. The single electron, time-independent Schrodinger equation is,

$$\left(-\frac{\hbar^2}{2m}\nabla^2 + V\right)\psi_n = E_n\psi_n, \quad (37)$$

where  $m$  is the appropriate effective mass ( $m_c^*$  for the conduction band,  $m_{hh}^*$  for the heavy hole valence band, or  $m_{lh}^*$  for the light hole valence band),  $V$  is the form of the potential, and  $\psi_n$  is the wave function of the  $n$ th level. The  $n$ th eigenenergy is given by  $E_n$  (for a specific band calculation,  $E_n \rightarrow E_{cn}, E_{hhn},$  or  $E_{lhn}$ ). We solve the time-independent Schrödinger equation in the dimension perpendicular to the plane of the quantum well, which we have designated as the  $y$ -direction. Assuming that the potential well is of the form,

$$V(y) = \begin{cases} 0 & \text{inside the well} \\ \Delta E & \text{outside the well} \end{cases} \quad (38)$$

where  $\Delta E$  is the appropriate band offset ( $\Delta E_c, \Delta E_{hh},$  or  $\Delta E_{lh}$ ) between the quantum well and the barrier material. This parameter is calculated assuming a conduction to valence band offset ratio of 3:2 for  $\text{Al}_x\text{Ga}_{1-x}\text{As}$  (barriers) to GaAs (quantum well) heterojunctions [14]. The wave function and its first derivative must be continuous across the heterojunction. Additionally, the wave function must go to zero far away from the well. The resulting solution, using (38) as the potential, is

$$\tan \left[ \frac{d_a}{2} \frac{\sqrt{2m(\Delta E - E_n)}}{\hbar} \right] = \left( \frac{\Delta E}{E_n} - 1 \right)^{-1/2} \quad n = 1, 3, 5, \dots, \quad (39)$$

$$\cot \left[ \frac{d_a}{2} \frac{\sqrt{2m(\Delta E - E_n)}}{\hbar} \right] = - \left( \frac{\Delta E}{E_n} - 1 \right)^{-1/2} \quad n = 2, 4, 6, \dots, \quad (40)$$

where  $d_a$  is the thickness of the well. These transcendental equations must be solved numerically for  $E_n$ . The solutions can be represented graphically by defining new parameters,

$$\eta \equiv \frac{d_a}{2} \frac{\sqrt{2m(\Delta E - E_n)}}{\hbar}, \quad (41)$$

$$\zeta \equiv \left( \frac{\Delta E}{E_n} - 1 \right)^{-1/2}. \quad (42)$$

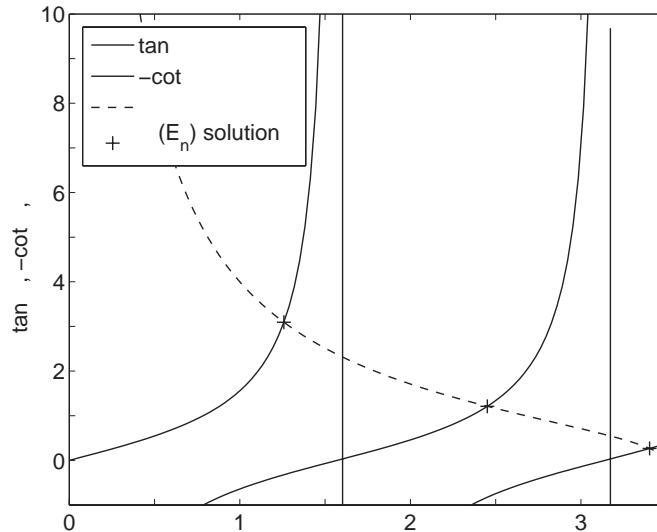


Figure 8: Graphical representation of the solution to Schrödinger's equation. The energy eigenvalues are the intersection of the  $\tan \eta$  and  $-\cot \eta$  curves with the  $\zeta$  curve. The solutions are indicated (in terms of  $\eta$ ) as + marks.

The graphical representation of the solution is shown in Fig. 8. The electron eigenenergy solutions are also plotted along with the conduction band through the well and barriers in Fig. 9. The optical wavelength is inversely proportional to the total difference in energy between the lowest conduction and valence sub-bands. Therefore, this calculation must be performed prior to the optical mode and gain calculations.

It is possible to couple the Poisson, Schrödinger, and current continuity equations [8], [11] in a semi-classical treatment, but this would require solving Schrödinger's equation at each iteration of the drift-diffusion solver. Therefore, following [14], the eigenenergies are calculated prior to the drift-diffusion module and are assumed to be decoupled.

## 6 Conclusion

A two-dimensional electrothermal model for high-powered diode lasers has been developed and discussed. A drift-diffusion model has been formulated to include recombination mechanisms relevant to a diode laser. A thermal model coupled to the drift-diffusion solver has been implemented to model the effects of temperature on electron-hole transport. An optical model has

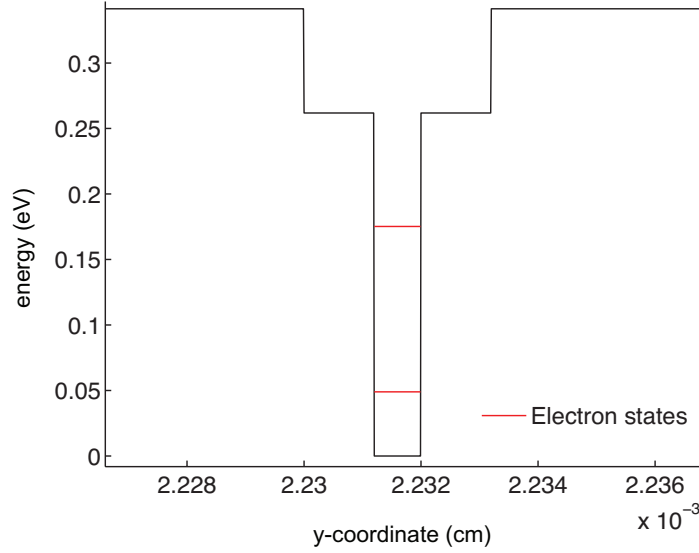


Figure 9: The allowed electron eigenenergies in an 8 nm GaAs quantum well (red) along with the conduction band profile through the y-direction.

been developed to determine the optical confinement factor, and therefore the portion of light absorbed by the waveguiding layers. Initial results for an asymmetric waveguide system have shown that the optical mode can be shifted into the n-doped cladding layer, which is less lossy than the p-doped cladding. Further, the coupling of the optical gain to the complex index of refraction used in the optical mode calculation has been discussed, as well as the relation of optical gain to the stimulated emission rate used in the drift-diffusion model. Lastly, a decoupled, one-dimensional quantum mechanical simulation has been solved to determine the energy states in the quantum well.

## Nomenclature

|   |   |
|---|---|
| $M_{QW}$                                    | Quantum well transition matrix element  |
| $\alpha_i$                                  | Internal losses   |
| $\Delta E_F$                                | Quasi-Fermi level separation  |
| $\Delta$                                    | Spin-orbit splitting energy   |
| $\Gamma$                                    | Optical confinement factor  |
| $\hbar$                                     | Reduced Planck constant, $\hbar = h/(2\pi)$   |
| $\kappa$                                    | Thermal conductivity  |
| $\lambda_0$                                 | Wavelength in vacuum  |
| $\mathcal{L}$                               | Lorentzian broadening function  |
| $\mu_n$                                     | Electron mobility   |
| $\mu_p$                                     | Hole mobility   |
| $\nabla \cdot, \nabla$                      | Divergence operator, gradient operator, respectively  |
| $\psi$                                      | Electrostatic potential   |
| $\psi_0$                                    | Equilibrium potential distribution  |
| $\rho_{red,j}$                              | Reduced density of states for $j^{th}$ conduction band  |
| $\tau_n$                                    | Shockley-Read-Hall relaxation time for electrons  |
| $\tau_p$                                    | Shockley-Read-Hall relaxation time for holes  |
| $\tau_{in}$                                 | Intraband relaxation time   |
| $\mathbf{E}_0$                              | Optical mode shape  |
| $\mathbf{j}_n$                              | Electron current density  |
| $\mathbf{j}_p$                              | Hole current density  |
| $\varepsilon_s, \varepsilon_0, \varepsilon$ | Relative static permittivity, vacuum permittivity, and absolute static permittivity, respectively |
| $\varphi_n$                                 | Electron quasi-Fermi potential  |

|               |  |
|---------------|--|
| $\varphi_p$   | Hole quasi-Fermi potential                                 |
| $c_0$         | Speed of light in vacuum                                   |
| $E_c$         | Conduction band minimum (bulk)                             |
| $E_F$         | Equilibrium Fermi energy                                   |
| $E_g$         | QW band gap  |
| $E_i$         | Photon energy  |
| $E_v$         | Valence band minimum (bulk)                                |
| $E_{cn}$      | $n^{th}$ quantized conduction band minimum                 |
| $E_{Fc}$      | Electron quasi-Fermi energy                                |
| $E_{Fv}$      | Hole quasi-Fermi energy                                    |
| $E_{jn}$      | $n^{th}$ quantized $j$ valence band minimum                |
| $f_{cn,j}$    | Modified Fermi distribution for conduction band            |
| $f_{vn,j}$    | Modified Fermi distribution for valence band               |
| $g$           | Optical gain   |
| $j$           | $j = hh, lh$ for heavy holes and light holes, respectively |
| $k_0$         | Wave number in vacuum                                      |
| $k_B$         | Boltzmann constant   |
| $L$           | Cavity length, perpendicular to the mirror planes          |
| $m^*$         | Modified effective mass                                    |
| $m_c^*$       | Conduction band density of states effective mass           |
| $m_v^*$       | Valence band density of states effective mass              |
| $M_{avg}$     | Bulk transition matrix element                             |
| $m_{hh}^*$    | Heavy hole effective mass                                  |
| $m_{lh}^*$    | Light hole effective mass                                  |
| $m_{red,j}^*$ | Reduced effective mass for the $j^{th}$ valence band       |

|                    |   |
|--------------------|---|
| $n$                | Electron concentration  |
| $N, N_D^+, N_A^-$  | Doping profile as a function of position, ionized donor concentration, ionized acceptor concentration, respectively |
| $N_c$              | Effective density of states for conduction band   |
| $n_i$              | Intrinsic carrier density   |
| $n_r, \bar{n}_r$   | Complex refractive index and its real part, respectively  |
| $N_v$              | Effective density of states for valence band  |
| $n_{g,\text{eff}}$ | Group effective refractive index  |
| $n_{N0}$           | Equilibrium electron concentration in the n-doped region  |
| $N_{ph}$           | Photon density  |
| $n_{r,\text{eff}}$ | Complex effective refractive index eigenvalue   |
| $n_{sp}$           | Population inversion factor   |
| $p$                | Hole concentration  |
| $p_{P0}$           | Equilibrium hole concentration in the p-doped region  |
| $q$                | Electron charge   |
| $q'''_{Joule}$     | Volumetric Joule heating  |
| $R$                | Recombination mechanisms  |
| $R_1, R_2$         | Mirror reflectivities   |
| $R'_{sp}$          | Spontaneous emission rate emitted into the lasing mode  |
| $R_{st}$           | Stimulated emission recombination rate  |
| $T$                | Temperature   |
| $T_{hs}$           | Heat sink temperature   |
| $V$                | Volume of the active region   |
| $V_a$              | Applied voltage   |
| $v_g$              | Group velocity of photons   |

## References

- [1] *COMSOL Multiphysics Model Library, version 3.5.*
- [2] Alfred R. Adams, Masahiro Asada, Yasuharu Suematsu, and Shigehisa Arai. The temperature dependence of the efficiency and threshold current of  $\text{In}_{1-x}\text{Ga}_x\text{As}_y\text{P}_{1-y}$  lasers related to intervalence band absorption. *Japanese Journal of Applied Physics*, 19(10):L621–L624, 1980.
- [3] M Asada, A Kameyama, and Y Suematsu. Gain and Intervalence Band Absorption in Quantum-Well Lasers. *IEEE Journal of Quantum Electronics*, 20(7):745–753, 1984.
- [4] M. Balkanski and R.F. Wallis. *Semiconductor Physics and Applications*. Oxford University Press, New York, New York, 2000.
- [5] J.S. Blakemore. *Semiconductor Statistics*. Dover Publications, Inc., Mineola, New York, 2002.
- [6] SR Chinn, PS Zory, and AR Reisinger. A Model for GRIN-SCH-SQW Diode-Lasers. *IEEE Journal of Quantum Electronics*, 24(11):2191–2214, Nov 1988.
- [7] Larry A. Coldren and Scott W. Corzine. *Diode Lasers and Photonic Integrated Circuits*. Wiley Series In Microwave and Optical Engineering. John Wiley & Sons, Inc., 1995.
- [8] EAB Cole, CM Snowden, and T Boettcher. Solution of the coupled Poisson-Schrodinger equations using the multigrid method. *International Journal of Numerical Modelling-Electronic Networks Devices and Fields*, 10(2):121–136, Mar-Apr 1997.
- [9] Roland Diehl, editor. *High-Power Diode Lasers: Fundamentals, Technology, Applications*. Springer-Verlag, Berlin, Germany, 2000.
- [10] S Gehrsitz, FK Reinhart, C Gourgon, N Herres, A Vonlanthen, and H Sigg. The refractive index of  $\text{Al}_x\text{Ga}_{1-x}\text{As}$  below the band gap: Accurate determination and empirical modeling. *Journal of Applied Physics*, 87(11):7825–7837, Jun 1 2000.
- [11] M. E. Grupen, U. Ravaioli, A. Galick, K. Hess, and T. Kerkhoven. Coupling the electronic and optical problems in semiconductor quantum well laser simulations. In W. W. Chow and M. Osinski, editors, *Society of Photo-Optical Instrumentation Engineers (SPIE) Conference*

- Series*, volume 2146 of *Society of Photo-Optical Instrumentation Engineers (SPIE) Conference Series*, pages 133–147, June 1994.
- [12] A Haug. Free-Carrier Absorption in Semiconductor-Lasers. *Semiconductor Science and Technology*, 7(3):373–378, Mar 1992.
- [13] Lin Li, Guojun Liu, Zhanguo Li, Mei Li, Hui Li, Xiaohua Wang, and Chunming Wan. High-efficiency 808-nm InGaAlAs-AlGaAs double-quantum-well semiconductor lasers with asymmetric waveguide structures. *IEEE Photonics Technology Letters*, 20(5-8):566–568, Mar-Apr 2008.
- [14] ZM Li, KM Dzurko, A Delage, and SP McAlister. A Self-Consistent 2-Dimensional Model of Quantum-Well Semiconductor-Lasers - Optimization of a GRIN-SCH SQW Laser Structure. *IEEE Journal of Quantum Electronics*, 28(4):792–803, Apr 1992.
- [15] K Mayes, A Yasan, R McClintock, D Shiell, SR Darvish, P Kung, and M Razeghi. High-power 280 nm AlGaIn light-emitting diodes based on an asymmetric single-quantum well. *Applied Physics Letters*, 84(7):1046–1048, Feb 16 2004.
- [16] Michael A. Morrison. *Understanding Quantum Physics: A User's Manual*. Prentice-Hall, Inc., Upper Saddle River, New Jersey, 1990.
- [17] Jayanta Mukherjee and John G. McInerney. Electrothermal analysis of CW high-power broad-area laser diodes: A comparison between 2-D and 3-D Modeling. *IEEE Journal of Selected Topics in Quantum Electronics*, 13(5, Part 1):1180–1187, Sep-Oct 2007.
- [18] Peter S. Zory, Jr., editor. *Quantum Well Lasers*, chapter 3, pages 141–145. *Quantum Electronics: Principles and Applications*. Academic Press, Inc., 1993.
- [19] NA Pikhtin, SO Slipchenko, ZN Sokolova, AL Stankevich, DA Vinokurov, IS Tarasov, and ZI Alferov. 16W continuous-wave output power from 100  $\mu$ m-aperture laser with quantum well asymmetric heterostructure. *Electronics Letters*, 40(22):1413–1414, Oct 28 2004.
- [20] M Rosenzweig, M Mohrle, H Duser, and H Venghaus. Threshold-Current Analysis of InGaAs-InGaAsP Multiquantum Well Separate-Confinement Lasers. *IEEE Journal of Quantum Electronics*, 27(6):1804–1811, Jun 1991.

- [21] B. S. Ryvkin and E. A. Avrutin. Free-carrier absorption and active layer heating in large optical cavity high-power diode lasers. *Journal of Applied Physics*, 100(2), Jul 15 2006.
- [22] Boris Ryvkin and Eugene Avrutin. Heating-induced carrier accumulation in the optical confinement layer and the output power in broadened symmetric and narrow asymmetric waveguide laser diodes. *Journal of Applied Physics*, 101(12), Jun 15 2007.
- [23] BS Ryvkin and EA Avrutin. Improvement of differential quantum efficiency and power output by waveguide asymmetry in separate-confinement-structure diode lasers. *IEE Proceedings-Optoelectronics*, 151(4):232–236, Aug 2004.
- [24] BS Ryvkin and EA Avrutin. Asymmetric, nonbroadened large optical cavity waveguide structures for high-power long-wavelength semiconductor lasers. *Journal of Applied Physics*, 97(12), Jun 15 2005.
- [25] BS Ryvkin and EA Avrutin. Effect of carrier loss through waveguide layer recombination on the internal quantum efficiency in large-optical-cavity laser diodes. *Journal of Applied Physics*, 97(11), Jun 1 2005.
- [26] BS Ryvkin and EA Avrutin. Nonbroadened asymmetric waveguide diode lasers promise much narrower far fields than broadened symmetric waveguide ones. *Journal of Applied Physics*, 98(2), Jul 15 2005.
- [27] M Sotoodeh, AH Khalid, and AA Rezazadeh. Empirical low-field mobility model for III-V compounds applicable in device simulation codes. *Journal of Applied Physics*, 87(6):2890–2900, Mar 15 2000.
- [28] Michal Szymanski. Two-dimensional model of heat flow in broad-area laser diode: Discussion of the upper boundary condition. *Microelectronics Journal*, 38(6-7):771–776, Jun-Jul 2007.
- [29] Dragica Vasileska and Stephen M. Goodnick. *Computational Electronics*. Morgan and Claypool Publishers, San Francisco, California, 2006.
- [30] RH Yan, SW Corzine, LA Coldren, and I Suemune. Corrections to the Expression for Gain in GaAs. *IEEE Journal of Quantum Electronics*, 26(2):213–216, Feb 1990.